Journal of the European Ceramic Society 7 (1991) 255–263

Fracture Toughness and Crack Bridging of a Silicon Nitride Ceramic

Y. Maniette,* M. Inagaki* & M. Sakai

Department of Materials Science, Toyohashi University of Technology, Tempaku-cho, Toyohashi 441, Japan

(Received 12 September 1990; accepted 16 November 1990)

Abstract

Toughening processes and mechanisms of a gas-pressure-sintered silicon nitride ceramic with β-phase rod-like microstructure are studied by the quantitative measurement of the R-curve in the form of the crack growth resistance, K_R, versus the crack extension, Δa, K_R being 4·3 $MPam^{1/2}$ at crack initiation and then increasing to 6·5 $MPam^{1/2}$ for its plateau value after a crack extension of about 1 mm. It is concluded that the toughness improvement of silicon nitride ceramics with rod-like microstructure arises from the crack bridging of the intact grains, but not from the crack-tip deflection and bowing processes which have been believed to date to be the key microfracture processes for toughening silicon nitride ceramics with ample rod-like β-phase grains.

An gasdruckgesintertem Si_3N_4 mit einem Gefüge aus stäbchenförmigem β-Si_3N_4 wurden durch quantitative Auswertung der R-Kurve wirkende Verstärkungsmechanismen untersucht. Dabei wurde der Rißwiderstand, K_R, über der Rißverlängerung, Δa, aufgetragen. Zu Beginn betrug der K_R-Wert 4·3 $MPam^{1/2}$ und stieg nach einer Rißausbreitung von circa 1 mm auf seinen Endwert von 6·5 $MPam^{1/2}$. Die Ergebnisse zeigen, daß die Zähigkeitssteigerung in Si_3N_4-Keramik mit stäbchenförmigem Gefüge auf eine Rißüberbrückung intakter Körner zurückzuführen ist. Dies widerspricht der bisherigen Annahme, die Zähigkeitssteigerung in Si_3N_4-Keramik mit β-Si_3N_4-Anteil durch durch eine Ablenkung an der Rißspitze oder einen Durchbiegungsprozeß zu erklären.

Nous avons étudié les mécanismes de renforcement d'une céramique de nitrure de silicium fabriquée par frittage sous pression de gaz, et caractérisée par la présence de gros cristaux aciculaires de β-Si_3N_4 en son sein. La mesure quantitative de la courbe R, montrant l'évolution du paramètre de résistance à la propagation des fissures, K_R, en fonction de l'extension de la fissure, Δa, nous a permis de relever une valeur à l'initiation de 4·3 $MPam^{1/2}$, et une valeur plateau de 6·5 $MPam^{1/2}$, atteinte après une croissance de 1 mm. Nous avons conclu que le renforcement des céramiques de nitrure de silicium à gros cristaux aciculaires est dû au pontage de la fissure par ces grains, et non pas à des phénomènes de déflection du front de fissure, qui jusqu'à présent étaient considérés comme le paramètre clé conduisant au renforcement des ceramiques de nitrure de silicium à gros cristaux de β-Si_3N_4.

1 Introduction

Ceramics have many attractive qualities including chemical durability, high hardness, wear resistance and high melting points. These properties are essential for the application of ceramics for engineering components utilized in extreme environmental conditions. Because of the nature of their brittleness, catastrophic failure under relatively low stress levels is a critical issue in the practical design of engineering structures with ceramics. Among various types of oxide and non-oxide ceramics, silicon

* Present address: Department of Applied Chemistry, Faculty of Engineering, Hokkaido University, Sapporo 060, Japan.

Journal of the European Ceramic Society 0955-2219/91/$3.50

nitride ceramics have received considerable interest during the last decade because of their promising mechanical and chemical properties, in addition to their relatively low density. These properties have been successfully applied to manufacturing high-speed rotating automobile turbocharger rotors. In this application, silicon nitride ceramics exhibit a superiority to SiC in the burst speed,[1] and to metals in the angular acceleration under constant torque.[2]

Because of the very low self-diffusion coefficient of silicon nitride[3] even at very high temperatures (>1500°C), either sintering aids are added to the starting powders, or the sintering is carried out by hot pressing[4] or under high-pressure nitrogen gas.[2] Of these three techniques, the last one may be the best for preparing engineering components with complicated shapes; furthermore the material keeps excellent mechanical properties at elevated temperature, probably due to the absence of amorphous phases at grain boundaries.[4,5]

The last decade has seen a dramatic upsurge of interest and improvement in the mechanical properties of engineering ceramics. These improvements have been made through the availability of highly pure and sinterable fine ceramic powders as well as by incorporating new toughening mechanisms such as fiber/whisker reinforcement, martensitic transformation, and stress-induced microcracking.

There are numerous microfracture mechanisms which occur in the frontal process zone ahead of a sharp crack, and contribute to the toughening of brittle ceramic materials.[6] These microfracture mechanisms 'shield' the crack tip from the far-field applied stresses. However, it has been recognized in recent years that the crack-tip shielding of brittle materials is perhaps more related to the microfracture mechanisms which occur behind the advancing crack tip in the following wake region as well as the contact area between the newly formed crack surfaces.[6] These shielding mechanisms include (a) crack-tip interactions (crack deflection, meandering and bowing), (b) zone shielding (dislocation, microcracking, phase-transformation, etc.), and (c) contact shielding (crack bridging and interlocking). Zone and contact shielding in the wake region generally enhance the rising crack growth resistance (rising R-curve) behavior for brittle materials. However, the crack-tip interactions through crack deflection, meandering and bowing, and various other crack impediment processes involving reinforcing elements (grains, whiskers, fibers) in addition to the microstructural local nonuniformity, do not generally promote rising R-curve behavior, because of the non-cumulative nature of their processes during the main crack extension.

The fracture toughness (K_{Ic}) of silicon nitride ceramics has been improved by developing rod-like grains of β-crystalline phase through a liquid-phase sintering process. A fracture toughness higher than 11 $MPam^{1/2}$ has already been reported in the literature.[7] These anisotropic grains in sintered silicon nitride ceramics have been considered to contribute to toughening through two distinct microfracture processes, i.e. toughening by crack deflection in the frontal zone and/or crack bridging of intact rod-like grains along the fracture surfaces behind the crack tip. It is readily expected that quantitative R-curve measurements should reveal which of these toughening processes is significant in silicon nitride ceramics with rod-like β-grains, because the crack deflection toughening by rod-like grains is not of a cumulative nature with regard to crack extension, and hence does not yield any rising R-curve behavior. However, few studies have been reported to date on the R-curve behavior of silicon nitride ceramics because of its very unstable crack extension.[8] Okada & Hirosaki[9] have reported a relationship between the R-curve and the texture of a silicon nitride ceramic, but their results failed to identify the specific toughening mechanism because of the R-curve complication associated with the chevron notches they used. On the other hand, some fractographic studies have been reported, although appropriate relationships between the fracture toughness and the microstructures have still not been established. Govila[10] has related the mechanical properties to the size of defects introduced by indentation with fractographic observations.

The intention of the present work is to disclose the toughening mechanisms of a silicon nitride ceramic with rod-like microstructure through R-curve measurement, and fracture toughness estimates by indentation microfracture techniques, and fractographic studies.

2 Experimental

2.1 Materials

The silicon nitride ceramic used in this work was provided by NTK Technical Ceramics Co. Ltd, as 80 × 80 × 3 mm plates. It was gas-pressure-sintered with alumina and yttria as sintering agents. Some properties at room temperature[8] include density of 3·21 g/cm^3, Young's modulus of 320 GPa, Vickers hardness of 14·3 GPa, three-point flexural strength of 1·1 GPa, and the fracture toughness measured by

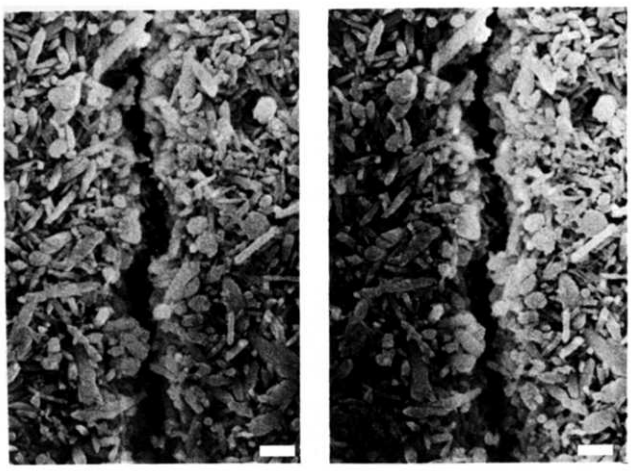

Fig. 1. Cracked and etched sample. Bar is 2 micrometers.

the single edge-precracked bend (SEPB) specimen is 6·5 MPam$^{1/2}$. The aspect ratio of the sintered rod-like grains ranges from 2 to 8, and the average diameter of the rod-like grains is about 0·8–1 μm. A scanning electron micrograph (SEM) of the ceramic surface etched by molten NaOH at 350°C for 5 min which typifies the microstructure is shown in Fig. 1. The X-ray diffraction analysis indicated that the ceramic contains about 90% β-Si_3N_4 and about 10% glassy phase localized at grain boundaries.

2.2 Indentation microfracture tests

The indentation microfracture technique (IM) and the indentation strength-in-bending test (ISB) were used to estimate the fracture toughness (K_{Ic}).[11,12] In the IM test, a diamond-polished 3-mm thick plate was indented on the stage of a commercial Vickers hardness tester (Akashi Co. Ltd, AVK-A II). The indentation-induced crack lengths ($2c$) were determined with the precision of $\pm 5\,\mu$m, where the test encompassed a relatively wide range of indentation loads (P_{ind}) from 10 to 200 N. The fracture toughness expression proposed by Anstis *et al.*[13] in the following form was adopted to estimate the K_{Ic} value:

$$K_{Ic} = 0{\cdot}016(E/H)^{1/2}(P_{ind}/c^{3/2}) \qquad (1)$$

where E and H are the Young's modulus and the Vickers hardness, respectively. The fracture toughness was actually estimated from the slope ($=[0{\cdot}016(E/H)^{1/2}/K_{Ic}]^{2/3}$) of the linear relationship between c/P_{ind} versus $P_{ind}^{-1/3}$ which must go through the origin of the graph, if the indentation-induced cracks are of the median/radical system.

In the ISB test, three-point bend specimens ($3 \times 3 \times 40$ mm) were indented in silicon oil by the Vickers indenter using the indentation loads, P_{ind}, from 10 to 300 N prior to fracture tests at room temperature in silicon oil by operating an Instron-type test machine (Sanwa Testing Machine Co. Ltd, Toyohashi, Japan) with a crosshead speed of 0·5 mm/min and a loading span of 30 mm. The K_{Ic} value was calculated by the expression[14] proposed by Chantikul *et al.*:

$$K_{Ic} = 0{\cdot}59(E/H)^{1/8}(\sigma_f \cdot P_{ind}^{1/3})^{3/4} \qquad (2)$$

where σ_f is the flexural strength of the indented bend specimen. The fracture toughness was estimated experimentally from the slope of the linear plot of σ_f versus $P_{ind}^{-1/3}$, which must extrapolate through the origin of the graph if the crack system is median/radial.

2.3 *R*-Curve measurement

The R-curve has been measured using a compact tension (CT) specimen with ASTM-E399 geometry,[15] with a specimen width, $W = 15{\cdot}6$ mm, height, $2H = 18{\cdot}7$ mm, thickness, $B = 0{\cdot}9$ mm, and an initial crack length, $a_0 = 11{\cdot}8$ mm. The notch was machined using a 0·3-mm thick diamond wheel and then precracked by about 3 mm using the crack stabilizer.[16] The precracked specimen was then renotched with a diamond blade, remaining about 10 μm-long sharp crack emanating from the diamond-sawed renotched tip. During the fracture test, the crosshead speed of the test machine was 5 μm/min. The crack extension (Δa) was monitored with a precision of $\pm 10\,\mu$m through a traveling microscope connected to a linear transducer. The crack growth resistance parameter, K_R, was then calculated by:[15]

$$K_R = PY(a/W)/(BW^{1/2}) \qquad (3)$$

where P is the critical load for the equilibrium crack, a is the crack length ($=a_0 + \Delta a$). The shape factor, $Y(\alpha)$, is expressed as:[15]

$$Y(\alpha) = [(2+\alpha)/(1-\alpha)^{3/2}] \times (0{\cdot}886 + 4{\cdot}64\alpha - 13{\cdot}32\alpha^2 + 14{\cdot}72\alpha^3 - 5{\cdot}6\alpha^4) \qquad (4)$$

where α is defined by a/W.

A stable crack extension which is always required for the R-curve measurement was successfully conducted by the use of a crack stabilizer[16] attached to the CT-specimen on the load line, as depicted in Fig. 2. The stabilizer absorbs the excessive elastic energy stored in the test machine, otherwise the excess energy leads to unstable crack extension for brittle ceramic specimens. The energy principle for crack extension behavior accompanied by stabilizers with different stiffness values has been thoroughly studied

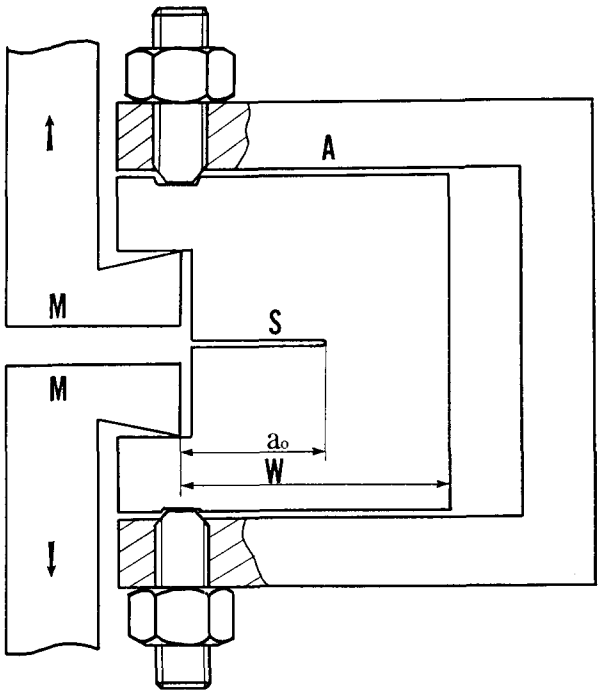

Fig. 2. Schematic test set-up including the loading fixture (M), test specimen (S), and the crack stabilizer (A).

by the present authors.[16] The stiffness of the stabilizer used in the present study was 10^7 N/m. Because of the extreme difficulty in stabilizing the crack extension of the silicon nitride ceramic used in this work, a compressive preload (10 N) was also applied to the CT-specimen on the load line by the screws of the stabilizer (see Fig. 2) prior to the *R*-curve measurement. The theoretical considerations of the effect of preloading on the crack extension stability are given in the Appendix.

2.4 Fractography

Stereographic microscopy of the fracture surfaces provides direct information on the microfracture processes (crack deflection and meandering, debonding at grain boundaries, grain bridging and pull-out), which are closely related to the observed *R*-curve behavior and toughening of the silicon nitride ceramic. Pairs of SEM micrographs for several spots of the fracture surfaces were prepared by tilting the specimen by $\pm\beta$ degrees using a commercial scanning electron microscope (JEOL Ltd, Tokyo, Japan, JSM-5200) by using magnification factors from 1000 to 20 000. The horizontal distances, D_h, and the vertical depths, D_v, in the photographed area were calculated by:

$$D_h = (d_1 + d_2)/2 \,.\, \cos\beta \quad (5)$$

$$D_v = (d_1 - d_2)/2 \,.\, \sin\beta \quad (6)$$

where d_1 and d_2 are the distances between two lines which are parallel to the rotation axis of the microscope sample holder, and pass through the considered points recorded on the photographs $1(d_1)$ and $2(d_2)$. The increase in the tile angle, β, not only increases the precision in depth measurements, but also enhances the stereoscopic effect of the micrographs as well.[17,18]

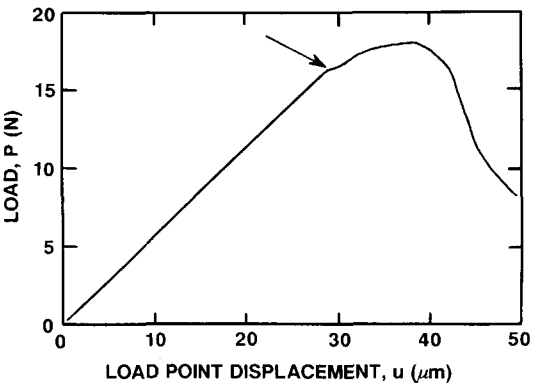

Fig. 3. Load versus load-point displacement curve. The arrow marks the onset point of crack propagation.

3 Results

The load (P) versus load-point displacement (u) curve is shown in Fig. 3. It demonstrates well a completely stable crack propagation. The arrow indicates the point of onset of the main crack extension. It should be noticed that the crack starts extension at a load somewhat lower than the peak load. This fact implies the rising behavior of the crack growth resistance.

The *R*-curve behavior in the form of K_R versus Δa is shown in Fig. 4. A characteristic of this fracture is a rising *R*-curve behavior at the initial stage of crack extension, followed by a toughness plateau region after the crack extension has reached about 1 mm. The true fracture toughness (K_{Ic}) which is defined at crack initiation ($\Delta a = 0$) is 4·3 MPam$^{1/2}$, and the

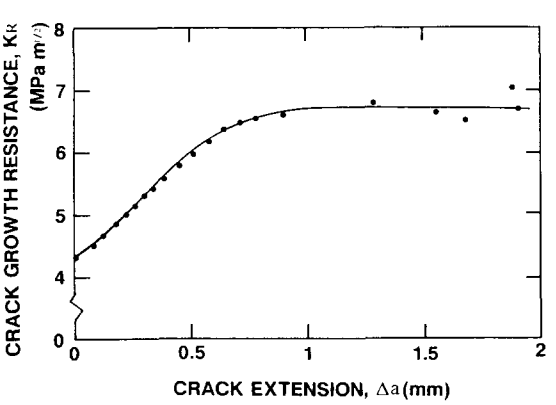

Fig. 4. Rising *R*-curve behavior of a gas-pressure-sintered silicon nitride ceramic.

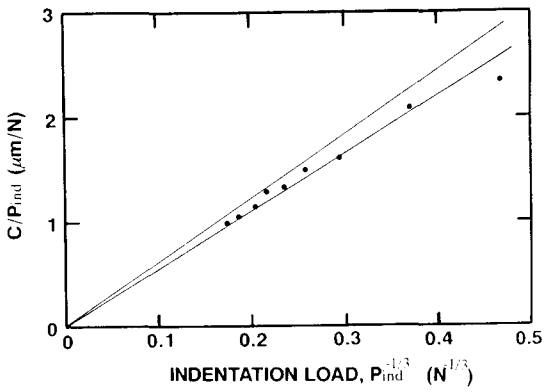

Fig. 5. Linear relationship between c/P_{ind} versus $P_{ind}^{-1/3}$ in the indentation microfracture test.

toughness value (K_R^r) in the plateau region is 6·5 MPam$^{1/2}$.

The results of the indentation microfracture tests (IM- and ISB-tests) are shown in Figs 5 and 6, respectively. The slopes of these linear plots yield the fracture toughness values as 6·2 ± 0·1 MPam$^{1/2}$, and 5·9 ± 0·4 MPam$^{1/2}$, respectively. These toughness values from the indentation microfracture tests are much closer to the K_R^r values than the true fracture toughness (K_{Ic}) determined in Fig. 4.

The SEM micrograph of the etched surface (Fig. 1) allows recognition and appreciation of the complicated microstructure of this ceramic. Most of the grains are small in diameter (0·2 μm); however, some grains are quite large (~ 2 μm). These observations are in fairly good agreement with the results obtained for the same material by Tajima *et al.*[8] They concluded the distribution of grain size had two broad peaks at about 0·4 and 1·2 μm.

Stereoscopic SEM micrographs of the fracture surface are shown in Fig. 7(a) to (c). A low magnification micrograph of the surface is shown in Fig. 7(a) for which a tilting angle of ±20° has been chosen. It is easily seen that there exist substantial crack/microstructure interactions, the fracture surface exhibiting a greater degree of tortuosity and grain pull-out, although the relatively high tilting angle used in these micrographs considerably enhances this tortuous appearance. Figure 7(b) ($\beta = \pm 10°$) shows a part of the same area demonstrated in Fig. 7(a), with evidence of rod-like thick grain pull-out of the order of 2 μm. This thick grain is oriented in a direction of about 45° with respect to the crack plane, as estimated from the stereoscopic SEM micrograph. The highly magnified 'socket' for this pull-out columnar grain is shown in Fig. 7(c). It shows a well-defined grain boundary debonding at

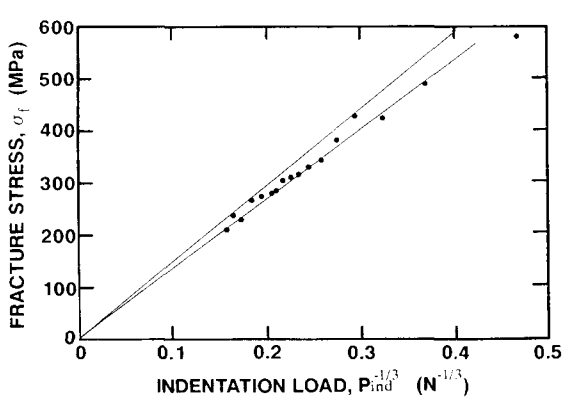

Fig. 6. Linear relationship between σ_f versus $P_{ind}^{-1/3}$ in indentation strength-in-bending test.

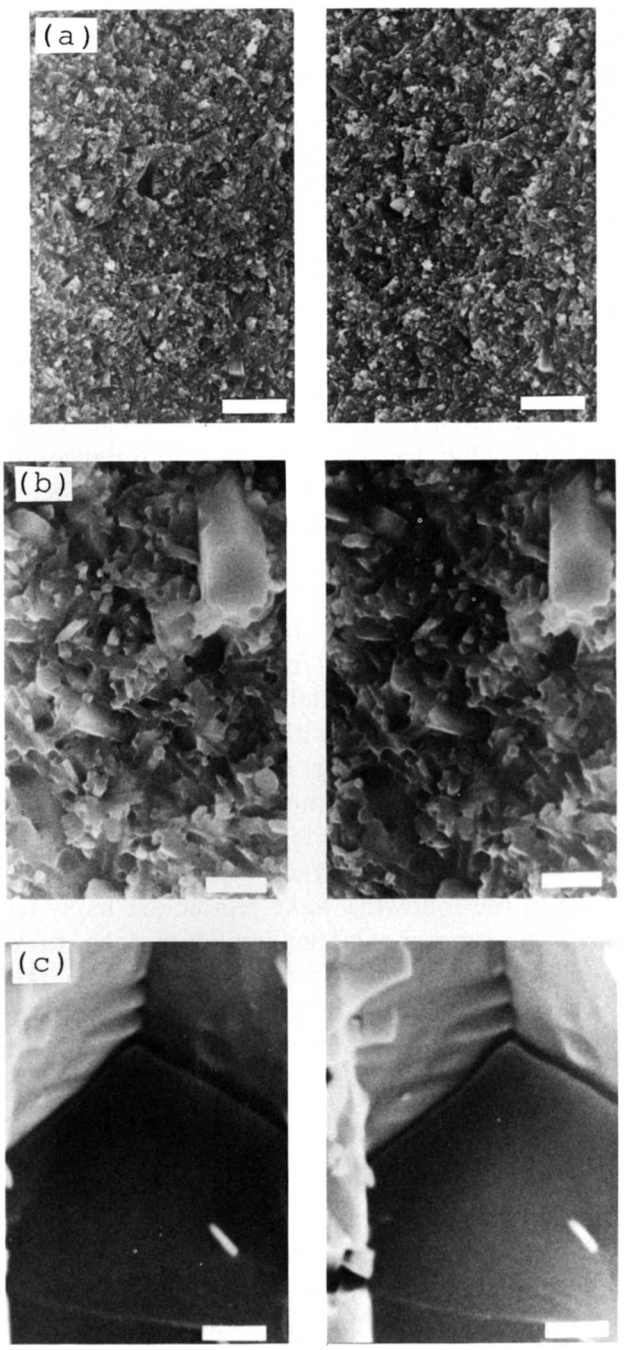

Fig. 7. SEM micrographs of a fracture surface. Bars are (a) 10, (b) 2 and (c) 0·5 micrometers.

the bottom of the 'socket'. It is hence clearly seen that the debonding crack extends further into the subsurface of the ceramic. The interface debonding may be induced during the sequence of 'grain boundary debonding–grain cracking–grain pull-out' microfracture processes which are associated with the main crack extension.[5]

4 Discussion

4.1 Rising *R*-curve and crack bridging

The rising *R*-curve in Fig. 4 provides the most substantial clue for considering the toughening processes and mechanisms of the present silicon nitride ceramic, since the K_{Ic}-value, from which the crack growth resistance (K_R) begins to increase with crack extension, is only 4·3 MPam$^{1/2}$, as mentioned in the foregoing section. In addition, it is very important to note that this fracture toughness value shows an excellent accordance with that of other silicon nitride ceramics with much finer sintered grains ($<1\ \mu$m in diameter) having a much smaller aspect ratio (<2), where none of the toughening processes, such as crack deflection in the frontal process zone as well as crack bridging and interlocking in the following wake region, are likely to occur.[8] This experimental fact implies that the crack tip deflection and bowing processes through the strong crack impediment by elongated β-phase grains are not essential for toughening the silicon nitride ceramic. However, the fractography illustrates the presence of significant crack/microstructure interactions such as crack plane interlocking and grain pull-out.

The toughness plateau (K_R^{∞}) of 6·5 MPam$^{1/2}$, which is attained after a crack extension of about 1 mm, thus cannot result from the crack deflection toughening, but arises from a grain bridging and interlocking process along the fracture surface behind the propagating crack tip.[6] It should be noticed that the toughness estimates by SEPB, IM and ISB techniques, which are always accompanied by some amount of crack extension before the toughness estimate, provide a good agreement between their fracture toughness values and the toughness plateau (K_R^{∞}) of the *R*-curve. In conclusion, the improved fracture toughness of silicon nitride ceramics with rod-like β-phase crystals arises from the crack bridging and interlocking in the wake region, but not from the crack-tip deflection process that has been believed to date to be the key microfracture process for the toughness improvement in silicon nitride ceramics with ample β-phase grains.

The toughening contribution derived from crack bridging is analyzed in terms of the effects of the formation of bridging zone on the stress intensity of the material utilizing the concept similar to a Dagdale zone model. When the bridging zone length, Δa, which is supposed to equal the crack extension is small compared with the total crack length, a, a corresponding result for the toughening contribution is given by:[19]

$$\Delta K(\Delta a) = (2/\pi)^{1/2} \int_0^{\Delta a} [\sigma_{br}(x)/x^{1/2}]\,dx \qquad (7)$$

where x is the distance from the crack tip, and $\sigma_{br}(x)$ is the bridging stress acting on the bridging zone. If the profile of $\sigma_{br}(x)$ versus x is assumed to remain the same within the bridging zone as the crack propagates, the differentiation of eqn (7) with respect to Δa yields the bridging stress as:

$$\sigma_{br}(\Delta a) = (\pi . \Delta a/2)^{1/2} [d(\Delta K(\Delta a)/ d(\Delta a)] \qquad (8)$$

It is easily seen from eqn (8) that the differentiation of the *R*-curve ($K_R(\Delta a)$ versus Δa relationship) with respect to the crack extension, Δa, gives the bridging stress for the ΔK as defined by $K_R(\Delta a) - K_{Ic}$.

The application of eqn (8) to the *R*-curve of the present silicon nitride ceramic (Fig. 4) is demonstrated in Fig. 8 in the form of σ_{br} versus Δa. The bridging stress is about zero at $\Delta a = 0$ mm, and then exhibits a strong increase in the initial stage of crack extension ($\Delta a < 0{\cdot}1$ mm), followed by a gradual increase to the maximum stress of about 90 MPa at $\Delta a = 0{\cdot}6$ mm. The subsequent crack extension results in the decrease in σ_{br}, which eventually becomes zero at $\Delta a (= \Delta a^*) \approx 1{\cdot}0$ mm, corresponding to the trailing edge of the steady-state bridging zone.

It is now possible to make the order of magnitude estimate of the crack-opening distance (ϕ^*) at the

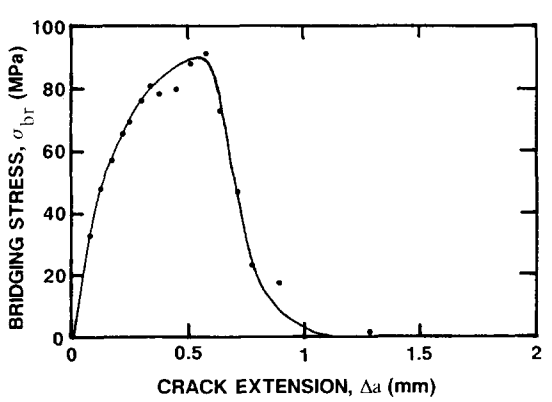

Fig. 8. Profile of crack bridging stress versus crack extension.

trailing edge from the numerical values of σ_{br} and Δa^* by the use of the following relationship:[20]

$$\phi^* = (8/E)(\Delta a^*/\pi)^{1/2}[\sigma_{br}(\Delta a^*/\pi)^{1/2} + K_{Ic}/2^{1/2}] \quad (9)$$

Substituting $\Delta a^* = 1{\cdot}0$ mm, $\sigma_{br} = 45$ MPa, and $K_{Ic} = 4{\cdot}3$ MPam$^{1/2}$ into eqn (9), the resulting value of ϕ^* is about 2·2 μm, in good agreement with the maximum pull-out length of the big rod-like grains observed in the SEM micrographs (Fig. 7(a) to (c)).

4.2 Microfracture processes and mechanisms

In the simplest fracture mode, a crack propagating through well-bonded brittle grains with rod-like shape might move through both grains and their boundaries, producing a very flat fracture surface, unlike the observation of the fracture surface of the present silicon nitride ceramic, where numbers of grains extruding from the fracture surface are appreciated and recognized (see Fig. 7(a)–(c)). The microfracture processes associated with the main crack extension of this ceramic are surmised as follows: The main crack front first interacts with randomly oriented rod-like grains. The crack is halted by this anisotropic grain, firstly because the higher stiffness along the rod-like grain axis inhibits further opening displacement of the main crack, and secondly because the strength of the grain is too high for it to fail by the current crack-tip stress field. As the load applied to the ceramic specimen is increased, the local stress near the crack tip begins to build up at the grain boundaries. The resistance to this local stress field at the grain interface is derived from the interface shear strength resulting not only from chemical bonding but also from the frictional shear strength of the interface by mechanical interlocking as well as by thermal mismatch compression. At some critical load the shear stress level developed at the interface will exceed the interface shear strength to result in local interface debonding at the grain boundary. This debonding moves along the grain boundary in both directions from the crack plane. However, if grain boundary debonding occurs in preference to main crack extension, it will not be a very high energy dissipating process, and cannot contribute very much to the total fracture energy. The effect of debonding, however, is to yield a substantial deviation of the crack tip parallel to the rod-like grain boundary, resulting in effective blunting of the main crack. Cracking may then move to some other plane away from the original crack plane, being referred to as 'crack-tip deflection', producing a resultant increase in the tortuosity of the fracture surface and crack/microstructure interaction. The crack-tip deflection toughening in the present silicon nitride ceramic through the crack impediment by β-phase rod-like grains, however, was proved not to be an important fracture process, as has been discussed in the preceding section.

After debonding, the rod-like grain and the surrounding grains 'matrix' move relative to each other to form crack bridging when crack opening continues. Some energy must be consumed against frictional resistance for this deformation and slip mode. Thus, the rod-like grain is subjected to a tensile stress over the debonding length. It may break at any point according to the Weibull statistics within the debonding length, or purely pulled out of the surrounding grains, if the debonding length exceeds the half length of the rod-like grain. It is very important to note the fact that the non-aligned, inclined rod-like grains typically fail by bending instead of pulling, and result in grain fracture without any grain pull-out, leading to no contribution to the fracture energy via the pull-out energy-consumption process.

After the failure of the rod-like grain, the broken ends are still gripped by the 'socket' of surrounding grains. It resists further crack opening, leading to ultimate failure of the ceramic specimen. Further frictional work (pull-out work) is required for this microfracture process. The decrease in the crack bridging stress (σ_{br}), which is shown in Fig. 8, after the crack extension of about 0·6 mm, may result from this grain pull-out process.

The toughening contribution from a steady-state crack bridging zone immediately behind the crack tip is approximated by

$$\Delta K (= K_R^{\infty} - K_{Ic}) = 2\sigma_{br}^0(2/\pi)^{1/2}(\Delta a^*)^{1/2} \quad (10)$$

after assuming a uniform bridging stress, σ_{br}^0. In eqn (10), Δa^* stands for the bridging zone length for steady-state cracking. The most substantial microfracture parameters for the crack bridging process are thus σ_{br}^0 and Δa^*. Noting the fact that σ_{br}^0 should be proportional to the strength (S) of the rod-like grain and that Δa^* should be proportional to the radius (R) of the grain,[21] eqn (10) can be recast into the following expression:

$$\Delta K = (\text{constant}).(S.R^{1/2}) \quad (11)$$

Equation (11) means that effective toughening by crack bridging can be attained by increasing both the grain strength (S) and the radius (R). The salient debonding and pull-out of a very thick grain

demonstrated in Fig. 7(b) and (c) confirm qualitatively the above discussion on the toughening process by crack bridging.

5 Conclusions

Toughening processes and mechanisms of a gas-pressure-sintered silicon nitride ceramic with β-phase rod-like microstructure have been addressed through the R-curve measurement, fracture toughness estimates by conventional fracture mechanics techniques and fractographic studies.

The K_{Ic} value, from which the crack growth resistance (K_R) begins to increase with crack extension (Δa), is 4·3 MPam$^{1/2}$, which is in good agreement with those for other silicon nitride ceramics with fine sintered grains ($<1\,\mu$m in diameter) and smaller aspect ratio (<2). The K_R value increased to its plateau value (K_R^{∞}) of 6·5 MPam$^{1/2}$ after a crack extension of about 1 mm. This toughness plateau was fairly close to the toughness values determined by the conventional SEPB, IM and ISB test methods. The inspection of the R-curve behavior as well as the SEM-fractography lead to the conclusions: (1) the toughness increment of the present silicon nitride ceramic with β-phase rod-like microstructure arises from the crack bridging and interlocking of the intact grains along the fracture surface behind the propagating crack tip, and (2) the crack-tip deflection and bowing processes which have been believed to date as the important toughening processes of this type of ceramics have no effects on the toughness improvement.

Acknowledgments

The authors are indebted to NTK Technical Ceramics Co. Ltd for preparing test samples. This work was supported by the Japanese Society for the Promotion of Science, Japanese Ministry of Education, and Engineering Research Association for High Performance Ceramics.

References

1. Wada, S., Masaki, A., Homma, T. & Tani, T., Injection molding of turbocharger rotors. In *Tokyo Ind. Gas Turbines Congress*, Tokyo, Japan, 26–31 October, 1987, pp. 143–7.
2. Hattori, Y., Tajima, Y., Yabuta, K., Matsuo, Y., Kawamura, M. & Watanabe, T., Gas pressure sintered silicon nitride ceramics for turbochargers applications. In *2nd Symposium on Ceramic Materials and Components for Engines*, Lubeck Travemunde, FDR, 14–17 April 1987.
3. Thummler, F., Sintering process. *Mat. Sci. Res.*, **13** (1980) 247.
4. Ukyo, Y. & Wada, S., High strength Si_3N_4 ceramics. *J. Japan. Ceram. Soc.*, **97** (1989) 872–4.
5. Evans, A. G., He, M. Y. & Hutchinson, J. W., Interface debonding and fiber cracking in brittle matrix composites. *J. Amer. Ceram. Soc.*, **72** (1989) 2300–3.
6. Green, D. J., Hannink, R. H. & Swain, M. V., *Transformation Toughening of Ceramics*. CRC Press, Florida, 1989, Chapter 3.
7. NKK Company, Products exhibited at the Nagoya Fine Ceramics Fair, Nagoya, Japan, 1990.
8. Tajima, Y., Urashima, K., Watanabe, M. & Matsuo, Y., Fracture toughness and microstructural evaluation of silicon nitride ceramics, *Ceram. Trans.*, Vol. 1, part B (1988) 1034–2.
9. Okada, A. & Hurosaki, N., Effect of microstructure on the R-curve behaviour of sintered silicon nitride. *J. Mater. Sci.*, **25** (1990) 1656–81.
10. Govila, R. K., Fracture phenomenology of a sintered silicon nitride ceramic containing oxide additives, *J. Mater. Sci.*, **23** (1988) 1141–50.
11. Ostojic, P. & McPherson, R., A review of indentation fracture theory. *Int. J. Fract.*, **33** (1987) 293–312.
12. Binner, J. P. G. & Stevens, R., The measurement of toughness by indentation. *Brit. Ceram. Trans. J.*, **83** (1984) 168–72.
13. Anstis, G. R., Chantikul, P., Lawn, B. R. & Marshall, D. B., A critical evaluation of indentation techniques for measuring fracture toughness. I: Direct crack measurements. *J. Amer. Ceram. Soc.*, **64** (1981) 533–8.
14. Chantikul, P., Anstis, G. R., Lawn, B. R., Marshall, D. B., A critical evaluation of indentation techniques for measuring fracture toughness. II: Strength method, *J. Amer. Ceram. Soc.*, **64** (1981) 539–43.
15. ASTM Standard E399-81. Annual book of ASTM standards, Part 10, American Society for Testing and Materials, Philadelphia, 1981.
16. Sakai, M. & Inagaki, M., Dimensionless load displacement relationship and its application to crack propagation problems. *J. Amer. Ceram. Soc.*, **72** (1989) 388–94.
17. Nankivell, J. F., Minimum differences detectable in height in electron stereomicroscopy. *Brit. J. Appl. Phys.*, **13** (1962) 126–8.
18. Wells, O. C., Correction of errors in electron stereomicroscopy. *Brit. J. Appl. Phys.*, **11** (1960) 199–201.
19. Hsueh, C. H. & Becher, P. F., Evaluation of bridging stress from R-curve behavior for non-transforming ceramics. *J. Amer. Ceram. Soc.*, **71** (1988) C234–C237.
20. Sih, G. C., *Handbook of Stress Intensity Factors*. Lehigh University Press, Bethlehem, PA, 1973, Section I.
21. Becher, P. F., Hsueh, C-H., Angelini, P. & Tiegs, T. N., Toughening behavior in whisker-reinforced ceramic matrix composites. *J. Amer. Ceram. Soc.*, **71** (1988) 1050–61.

Appendix

A general principle of crack extension stability has been considered by the present authors[16] in the form of dimensionless Gibbs free energy of the test system, and has been applied to the condition for the crack extension stability of a fracture mechanics test specimen with a crack stabilizer (see Fig. 2). In the present fracture test, a compressive preload was applied to the load line to enhance the stability of the crack extension during the R-curve measurement.

The total energy ($\tilde{G}_{eq}(\alpha)$) of the fracture test system in dimensionless form is given by

$$\tilde{G}_{eq}(\alpha) = \tilde{G}_s(\alpha) + \tilde{G}_a + \tilde{G}_m \quad \text{(A1)}$$

where α is the relative crack length (a/W), and $\tilde{G}_s(\alpha)$, $\tilde{G}_a$ and $\tilde{G}_m$ are the total energy of the test specimen including fracture surface energy, elastic stored energies of the stabilizer and the test machine, respectively. The compressive preload prior to the fracture test mirrors the crack extension stability through the following energy expression;

$$\begin{aligned}\tilde{G}_{eq}(\alpha) = {} & \tilde{G}^0_{eq}(\alpha) \\ & + \tilde{u}(\alpha)\tilde{u}_0(S_s/S_m)[S(\alpha) + S_s + S_m] \\ & + (1/2)\tilde{u}_0^2(S_s/S_m)(S_a + S_m)\end{aligned} \quad \text{(A2)}$$

where $\tilde{G}^0_{eq}(\alpha)$ is the total energy of the test system in the absence of preload, and has been given in Ref. 16. The dimensionless stiffnesses, $S(\alpha)$, S_s, and S_m for the test specimen, the stabilizer and the test machine are, respectively, defined by $k(\alpha)/BE'$, k_s/BE', and k_m/BE' using their stiffnesses, ($k(\alpha)$, k_s, k_m), the specimen thickness (B) and the specimen elastic modulus (E'). The specimen displacement, $\tilde{u}(\alpha)$, and the stabilizer displacement by the preload, $\tilde{u}_0$, in dimensionless forms are defined by $u(\alpha)E'/K_cW^{1/2}$ and $p_0[\{S(\alpha_0)+S_s\}/S_sS(\alpha)]/K_cW^{1/2}$, respectively, using the load-point displacement of the specimen ($u(\alpha)$), preload (p_0), the specimen fracture toughness (K_c) and the specimen width (W). It can be readily shown that the second term on the right-hand side of eqn (A2),

$$\tilde{u}(\alpha)\tilde{u}_0(S_s/S_m)[S(\alpha) + S_s + S_m]$$

must increase with increasing relative crack length, α, i.e. with incremental crack extension, provided that the preload is effective for the crack extension stability. In other words, the sign of the derivative of this second term must be positive with respect to α for the preloaded stabilizer to enhance the crack extension stability, i.e.

$$S_s + S_m > Y'(\alpha)/[\lambda'(\alpha)Y(\alpha) - \lambda(\alpha)Y'(\alpha)] \quad \text{(A3)}$$

where use has been made of the following relationships:

$$\lambda(\alpha) = C(\alpha)BE'$$

$$\tilde{u}(\alpha) = \lambda(\alpha)/\mathrm{Y}(\alpha)$$

$$Y'(\alpha) = \mathrm{d}\,Y(\alpha)/\,\mathrm{d}\alpha$$

$$\lambda'(\alpha) = \mathrm{d}\lambda(\alpha)/\,\mathrm{d}\alpha$$

where $C(\alpha)$ is the specimen compliance, and the parameters $\lambda(\alpha)$ and $Y(\alpha)$ are the dimensionless compliance and the stress intensity factor of the test specimen, respectively.